G. Vlad

europhysics conference abstracts

18th European Conference on

Controlled Fusion and Plasma Physics

Berlin, 3-7 June 1991

Editors: P. Bachmann, D.C. Robinson

Contributed Papers
Part IV

Published by: European Physical Society

Series Editor: Prof. K. Bethge, Frankfurt/M.

Managing Editor: G. Thomas, Geneva

VOLUME
15 C
Part IV

FREE BOUNDARY TOROIDAL STABILITY OF IDEAL AND RESISTIVE INTERNAL KINKS

G. VLAD, Associazione Euratom-ENEA sulla Fusione, C.R.E. Frascati
C.P. 65-00044 -Frascati, Rome, Italy

H. LUTJENS, A. BONDESON, Centre de Recherches en Physique des Plasmas, Association Euratom - Confédération Suisse, Ecole Polytechnique Fédérale de Lausanne, 21 Av. des Bains, CH-1007 Lausanne, Switzerland

I. INTRODUCTION

Recently, there has been a strong interest in the stability properties of the internal kink mode. This has been spurred mainly by experimental observations of sawtooth oscillations on large tokamaks revealing unexpected features such as double sawteeth with partial reconnection, fast crashes, and central q-values well below unity [1]. These observations are all difficult to reconcile with the conventional Kadomtsev model in which the crash is triggered by the resistive kink mode becoming unstable when the safety factor q falls below unity. The theoretical understanding of the sawtooth activity is made difficult by the sensitivity of the internal kink mode to several factors such as q-profile, pressure, resistivity, aspect ratio, shaping of the cross-section, and even wall position. In addition, the internal kink in a torus (with $q > 1/2$) is a rather weak instability and should therefore be sensitive to kinetic effects.

Here, we present results from a study of the resistive and ideal MHD properties of the internal kink mode. Generally, we have numerically computed growth-rates as functions of various parameters, using the full-resistive-MHD toroidal stability code MARS [2] and the cubic element equilibrium code CHEASE [3].

II. INFLUENCE OF THE CURRENT PROFILE

A major uncertainty for the understanding of the sawteeth is the shape of the current profile. Here, we restrict attention to circular cross-section with an aspect ratio of 4 and choose two types of current profiles. One has uniformly low shear inside a certain radius $r = r_p = 0.4a$, outside which the shear increases rapidly. The other has shoulders in the current profile which produce locally low shear near $q = 1$, while the central safety factor q_0 is well below unity. We refer to these as "low-shear" and "TEXTOR" profiles [1], respectively.

Figure 1 shows the low-shear current profile $j = \langle j_\phi \rangle(r)$ (where r is a flux surface label proportional to the square root of the enclosed volume). This current profile is monotone, but the shear $\hat{s} = (r/q)\, dq/dr$ has a slight local minimum at $r = r_p \approx 0.4a$, $\hat{s}(r_p) \approx 0.03$. The shear does not exceed 0.032 in the entire region $r < r_p$. Profiles of this type may arise in sawtoothing discharges if total reconnection occurs within the $q = 1$ region, $r < r_p$, followed by neoclassical peaking of the current during the rise phase [4]. We have considered a family of equilibria with self-similar current profiles where we specify the q-value at radius $r = r_p$. For this family, the central safety factor q_0 is related to $q_p \equiv q(r_p)$ by $q_0 \approx 0.948 q_p$. It may be useful to think of these equilibria as an approximation to the sequence in time during the ramp phase of a sawtooth, with q_0 and q_p decreasing functions of time. Figure 2 shows the resulting growth-rates for four different values of poloidal beta at the $q = 1$ surface (0.00, 0.05, 0.10, and 0.15) at Lundquist number $S \equiv \tau_{res}/\tau_A = 10^6$ (Fig 2a), 10^8 (2b) and 10^{10} (2c). For this q-profile, $q_p = 1$ locates the minimum shear ($s \approx 0.03$) at the $q = 1$ surface, and when q_p is decreased below unity, the $q = 1$ surface moves out into the region of high shear. For instance, $q_p = 0.98$ gives $\hat{s}(q{=}1) \approx 0.22$. In all cases shown in Fig. 2, a conducting wall is assumed at $r = b = 1.2a$.

We note from Fig. 2 that *complete* resistive MHD stability is very rarely achieved. However, in many cases, the resistive growth-rates are small, and we are led to the conclusion that a weak internal kink is stabilized for most of the sawtooth cycle by effects not included in the model. A likely candidate for such stabilization is diamagnetic rotation. In present day tokamaks, ω_*/ω_A is typically between 0.5×10^{-3} and 10^{-2}, which is comparable to resistive

MHD growth-rates of the internal kink. It therefore appears plausible that diamagnetic rotation can stabilize the internal kink as long as its resistive-MHD growth-rate is not too large.

By comparing Figs. 2a-c for different values of S, we note a gradual change in the main factor determining the growth-rate. At $S = 10^6$, the growth-rates are mainly dependent on q_p, i.e., on the shear at the q = 1 surface, and are only weakly dependent on the pressure. This is typical of the resistive kink mode. This picture is modified somewhat at $S = 10^8$ which represents an intermediate case. The three lower curves in Fig. 2b ($\beta_{pol} = 0.00, 0.05, 0.10$) still show reasonably high growth-rates (about $2 \times 10^{-3}\ \omega_A$) for a current driven resistive mode, but for $\beta_{pol} \leq 0.1$, the pressure has only a weak influence on the growth-rates. For $\beta_{pol} = 0.15$, destabilization by pressure becomes significant. An interesting aspect of this "pressure driven" instability is that it is clearly sensitive to the q-profile and its growth-rate rises sharply when the q = 1 surface moves out into the region of high shear. Thus, although the instability is *pressure driven*, it can be thought of as being *triggered* by the *current profile*.

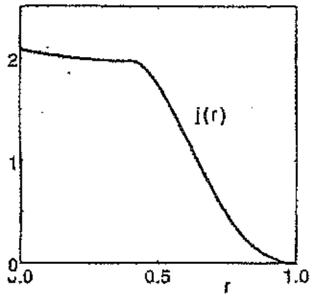

Figure 1. *Low-shear current profile*

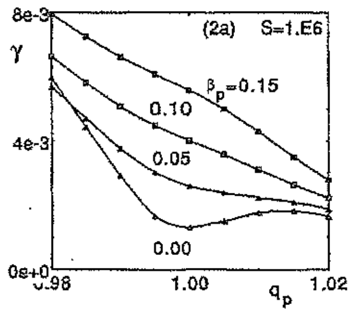

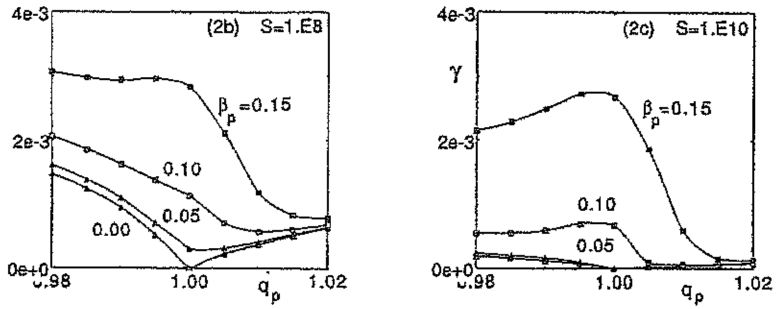

Figure 2. *Resistive growth-rates for low-shear current profile and different β_{pol}*

Much more clear changes from the low-S picture are seen in Fig 2c for $S = 10^{10}$. Here, the resistive growth-rates for $\beta_{pol} = 0.00$, and 0.05 are rather small (a few times $10^{-4}\ \omega_A$) and the pressure driven instability is clearly dominant. Comparing the growth-rates with those for $S = 10^8$, we see that the pressure driven instability is essentially ideal. Thus, it appears that as S is increased, the linear instability leading to the sawtooth crash becomes more and more an ideal, pressure driven instability. However, *this ideal mode is sensitive to details of the current profile and can be triggered by a slight shift in the q-profile.* In fact, the variation of the growth-rate with q_p at high S and not-too-small β_{pol} is more pronounced than for the resistive kink mode at low S. Figure 2c also shows that the critical β_{pol} for ideal stability is rather low, about 0.1 for this current profile. We have obtained results similar to those in Fig. 2 for a current profile with twice the shear in the central region. In this case, the resistive mode at low pressure gives somewhat higher growth-rates than the low-shear case shown in Fig. 2.

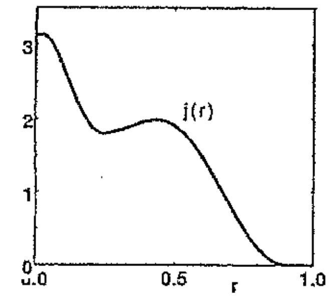

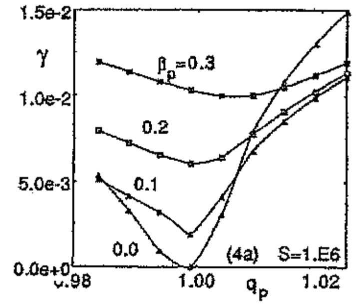

Figure 3. *TEXTOR current profile*

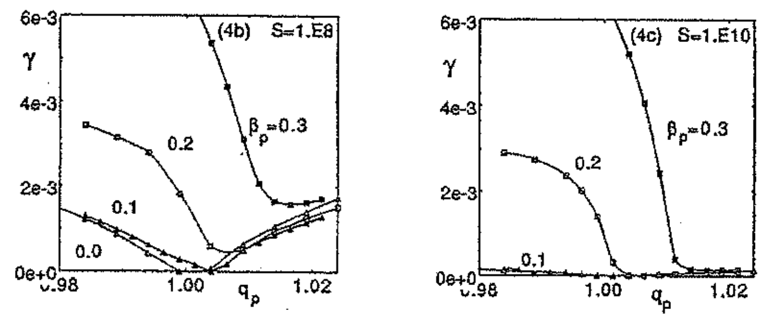

Figure 4. *Resistive growth-rates for TEXTOR current profile and different β_{pol}*

We have also computed resistive growth-rates for a current profile of TEXTOR type, as shown in Fig. 3. The shoulders in the current profile were adjusted so that the shear has a minimum of about 0.034 at $r = r_p \approx 0.44a$. In this case, the global shear in the central region is strong and $q_0 = 0.634 q_p$ is well below unity. Figure 4 shows the growth-rates for different S-values and $\beta_{pol} = 0.0, 0.1, 0.2,$ and 0.3. In general terms, the behavior is similar to that for the low-shear profile, but the TEXTOR profile supports about twice the pressure before becoming ideally unstable.

III. WALL AND SHAPING EFFECTS

Although the displacement of the internal kink mode is mainly localized to the region inside the q = 1 surface, the magnetic perturbation outside q = 1 is not small and it is important for the mode stability [5]. Numerically, we find that the ideal stability boundaries are strongly influenced by wall position when the q = 1 radius is sufficiently large and the aspect ratio is low. As an example, Fig. 5a shows growth-rates for the ideal internal kink as a functions of β_{pol} at q=1 for a sequence of circular equilibria with $r_{q=1}/a = 0.6$ and edge q between 2 and 3. Two different wall positions have been considered: b/a = 1 (fix boundary) and b/a = 2 (free boundary). For this equilibrium, we find that the difference in marginal β_{pol} between the fix and free boundary cases scales as the square of the inverse aspect ratio, as expected from large aspect ratio theory. At low aspect ratio, the wall position plays a significant role; the marginal β for free boundary stability is only about half of the fixed boundary value for R/a = 2.7. When the edge q is raised above 3 for the circular equilibrium, the influence of the wall position is weak and not of practical significance.

In the case of shaped cross-section and a large q = 1 surface, the wall position has a more dramatic influence. An example is shown in Fig. 5b for JET-shaped cross-section with elongation κ = 1.7 and triangularity δ = 0.3. The aspect ratios are A = 3.5, 6, and 10, respectively, and $r_{q=1} = 0.6a$ and $q_0 = 0.7$ are held fixed. The edge q varies with aspect ratio but remains between 3 and 4. For this equilibrium, the wall has a strong influence independent of the aspect ratio. Note that for A > 4.5, the equilibrium is free-boundary unstable even at zero beta. This, too, is in agreement with large aspect ratio theory, as δW contains stabilizing terms $\approx (r_{q=1}/R)^2$ and destabilizing terms $\approx (\kappa-1)^2$. Thus, at fixed κ > 1, large aspect ratio theory predicts instability even at zero beta when the aspect ratio is sufficiently large. Triangularity has a stabilizing influence, but for JET geometry and the q-profile used here, this stabilization is insufficient to compensate for the destabilization by ellipticity.

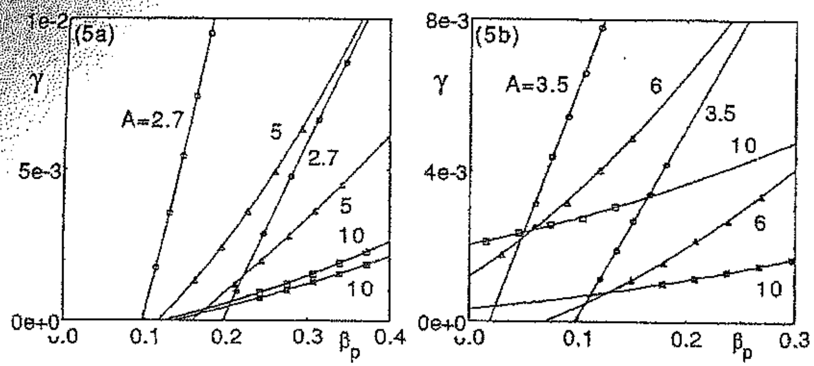

Figure 5. *Ideal growth-rates for free and fixed boundary at different aspect ratios. Free boundary is indicated by open symbols. (a) Circular and (b) JET cross-section*

REFERENCES

1. H. Soltwish, W. Stodiek, J. Manickam, *et al*, IAEA Kyoto (1986), Vol I, p. 263.
2. A. Bondeson, G. Vlad and H. Lütjens, EPS Amsterdam (1990), Vol. II, p.906.
3. H. Lütjens, A. Bondeson, and A. Roy, LRP 405/90, submitted to Comput. Phys. Comm.
4. W. Park and D.A. Monticello, Nucl. Fusion 30, 2413 (1990).
5. M.N. Bussac, R. Pellat, D. Edery and J.L. Soule, Phys. Rev. Lett. 35, 1638 (1975).

COMPUTING THE DAMPING AND DESTABILIZATION OF GLOBAL ALFVÉN WAVES IN TOKAMAKS

W. Kerner, S. Poedts*, J.P. Goedbloed**,
G.T.A. Huysmans**, B. Keegan, and E. Schwarz*

JET Joint Undertaking, Abingdon, OXON., OX143EA, UK
* Max-Planck Institut für Plasmaphysik, Garching, Germany
** FOM-Instituut voor Plasmafysica, Nieuwegein, The Netherlands

The role of ideal MHD in magnetic fusion is in the first place to discover magnetic geometries with favourable equilibrium and stability properties. Non-ideal effects cause slower and weaker instabilities leading to enhanced transport and often to violent disruptions.

MHD spectroscopy, i.e. the identification of ideal and dissipative MHD modes for the purpose of diagnosing tokamaks and optimising their stability properties, requires a numerical tool which accurately calculates the dissipative MHD spectra for measured equilibria. The new spectral code CASTOR (Complex Alfvén Spectrum for TORoidal Plasmas), together with the equilibrium solver HELENA [1], provides such a tool. In CASTOR, the fluid variables ρ, **v**, T, and **b** are discretized by means of a combination of cubic Hermite and quadratic finite elements for the radial direction and Fourier modes for the poloidal coordinate. The equilibrium in non-orthogonal flux coordinates ψ, θ, φ with straight field lines is computed using isoparametric bicubic Hermite elements, resulting in a very accurate representation of the metric elements. Finally, for analysis of JET discharges the equilibrium solver HELENA is interfaced with the equilibrium identification code IDENTC(D).

All quantities are expanded around an axisymmetric equilibrium ($\partial/\partial\phi = 0$) in the form

$$f(r,t) = f_0(s,\theta) + e^{\lambda t} e^{in\phi} f_1(s,\theta), \quad \text{with} \quad s = \sqrt{\psi/\psi_s}. \tag{1}$$

Here, λ is the eigenvalue. The imaginary part of λ corresponds to oscillatory behaviour, while a negative real part yields damping and a positive real part yields an exponentially growing instability. With resistivity η, the equations for the perturbed density ρ, velocity **v**, temperature T, and vector potential **a** in normalised units read

$$\lambda \rho = -\nabla\cdot(\rho_0 \mathbf{v}), \tag{2a}$$

$$\lambda \rho_0 \mathbf{v} = -\nabla(\rho_0 T + T_0 \rho) + (\nabla\times\mathbf{B}_0)\times\mathbf{b} + (\nabla\times\mathbf{b})\times\mathbf{B}_0 - \nabla\cdot\Pi, \tag{2b}$$

$$\lambda \rho_0 T = -\rho_0 \mathbf{v}\cdot\nabla T_0 - (\gamma-1)\rho_0 T_0 \nabla\cdot\mathbf{v}, \tag{2c}$$

$$\lambda \mathbf{a} = \mathbf{v}\times\mathbf{B}_0 - \eta_0 \nabla\times\nabla\times\mathbf{a}, \quad \text{where} \quad \mathbf{b} = \nabla\times\mathbf{a}. \tag{2d}$$

The pressure tensor Π contains the influence of the anisotropic bulk plasma and of the energetic ions interacting with the fluid. The latter requires the solution of the linearised Vlasov equation for both trapped and passing particles yielding a complicated dependence on λ.